Particle & Particle Systems Characterization
www.particle-journal.com

Metal–Drug–Protein Assemblies: Gd^{3+} Self-Enhanced Magnetic Resonance Imaging, High-Sensitive Tumor-Targeting Imaging and Efficient Chemo-Phototherapy

Jia Zhou, Tianliang Li, Yiran Zhang, Xiaoyu Xu, Chunlei Zhang, Yuehua Li, Daxiang Cui, and Yingsheng Cheng**

Magnetic resonance imaging (MRI) contrast agents are broadly employed for better clinical trials in MR imaging. Magnevist solution (Gd-DTPA), a clinical MRI contrast agent, possesses inherent shortcomings like poor r_1 relaxation, short half-time, nephrotoxicity, etc. To overcome these problems, Gd-DTPA-grafted protein assemblies (Gd-P-ABs) loading with anticancer drug cisplatin and photosentizer IR-780 are constructed via chelation of Gd^{3+}. Gd-P-ABs exhibit dual MR/fluorescence (FL) imaging–guided chemo/photothermal therapy. Interestingly, Gd-P-ABs behave as aggregation-enhanced magnetic resonance imaging with an extremely high r_1 value of 26.391 s^{-1} mM^{-1}, which is about 5.5-fold larger than Gd-DTPA (≈4.8 s^{-1} mM^{-1}). Consequently, better MRI performance is presented with the same concentration of Gd ions. When exposed to acidic tumor microenvironment and light irradiation, Gd-P-ABs show significant drug release capacity. Good cell killing ability in vitro is also determined due to effective folate-targeting ability and high photo–heat conversion. In vivo MR/FL imaging results reveal that Gd-P-ABs possess high-sensitivity tumor-targeting imaging and long tumor retention, which are attributed to the folate-targeting ability and small size effect. Combined chemo/photothermal therapy in vivo demonstrates that the tumor can be eventually ablated. Altogether, the Gd-P-ABs possess great potential for clinical imaging-guided tumor therapy.

1. Introduction

Magnetic resonance imaging (MRI) is a powerful and noninvasive imaging technique for tumor detecting with high spatial resolution and unlimited tissue penetration.[1–3] For better diagnosis, MRI contrast agents are usually utilized to shorten the T_1 relaxation (positive) time or T_2 relaxation (negative) time.[4–6] Magnevist solution (Gd-DTPA), a clinic MRI contrast agent, has some shortcomings, such as nonselectivity, low r_1 relaxation, and short imaging time. Therefore, to realize better diagnosis usually required large amount of Gd ions. The potential risks of nephrogenic systemic fibrosis in patients are worrying.[7–9] However, due to lack of alternative MRI agent, so far, magnevist is still the most common used for T_1-weighted MR imaging in clinic. To overcome the limitation, Gd ion–based nanomaterials can provide effective solution. Xing et al. have reported that a kind of Gd-DTPA-modified bovine serum albumin (BSA) complex, it has a larger T_1 relaxivity (r_1) than Gd-DTPA.[10] Hou et al. have reported that self-assembly of gold nanocluster induced by Gd ions behaved enhanced T_1-weighted MR performance.[11] Wang et al. have reported that albumin-based gadolinium oxide (Gd_2O_3) nanocrystals which exhibited lager relaxivity (12.3 mM^{-1} s^{-1}, 1.5 T) than Gd-DTPA (3.2 mM^{-1} s^{-1}, 1.5 T).[12] Inspired by the above strategies, a new kind of Gd^{3+}-based nanomaterials with excellent T_1-weighted MR performance means useful.

Furthermore, by integration of contrast agents and drug agents, imaging-guided therapy strategy has been broadly employed into advanced drug delivery systems for cancer diagnosis and therapy.[13–16] It could offer more accurate localization of the tumor and realize synergistic therapy effects than a single one.[17,18] Up to day, many kinds of nanoplatforms have been explored for imaging-guided cancer therapy.[19,20] However, in the progress of fabricating an all-in-one nanoplatform, it is either difficult to integrate the agents together or resulted in poor stability and biocompatibility by simply mixing.[21–23] Therefore, a suitable drug carrier is a key issue to complete an excellent multifunctional nanoplatform.

Albumin, one of the most abundant proteins, has played versatile roles in drug delivery due to its good biocompatibility and easy-grafted groups. Numerous publications have reported that albumin can act as a drug carrier,[24–26] reactor,[12,27]

Dr. J. Zhou, Y. Zhang, X. Xu, Prof. Y. Li, Prof. Y. Cheng
Department of Radiology
Shanghai Jiao Tong University Affiliated Sixth People's Hospital
600 Yishan Road, Shanghai 200233, China
E-mail: liyuehua312@163.com; chengyingsheng@hotmail.com
Dr. T. Li, Dr. C. Zhang, Prof. D. Cui
Institute of Nano Biomedicine and Engineering
Shanghai Engineering Research Center for Intelligent Instrument for Diagnosis and Therapy
Department of Instrument Science & Engineering
School of Electronic Information and Electrical Engineering
Shanghai Jiao Tong University
800 Dongchuan Road, Shanghai 200240, China
The ORCID identification number(s) for the author(s) of this article can be found under https://doi.org/10.1002/ppsc.201900427.

DOI: 10.1002/ppsc.201900427

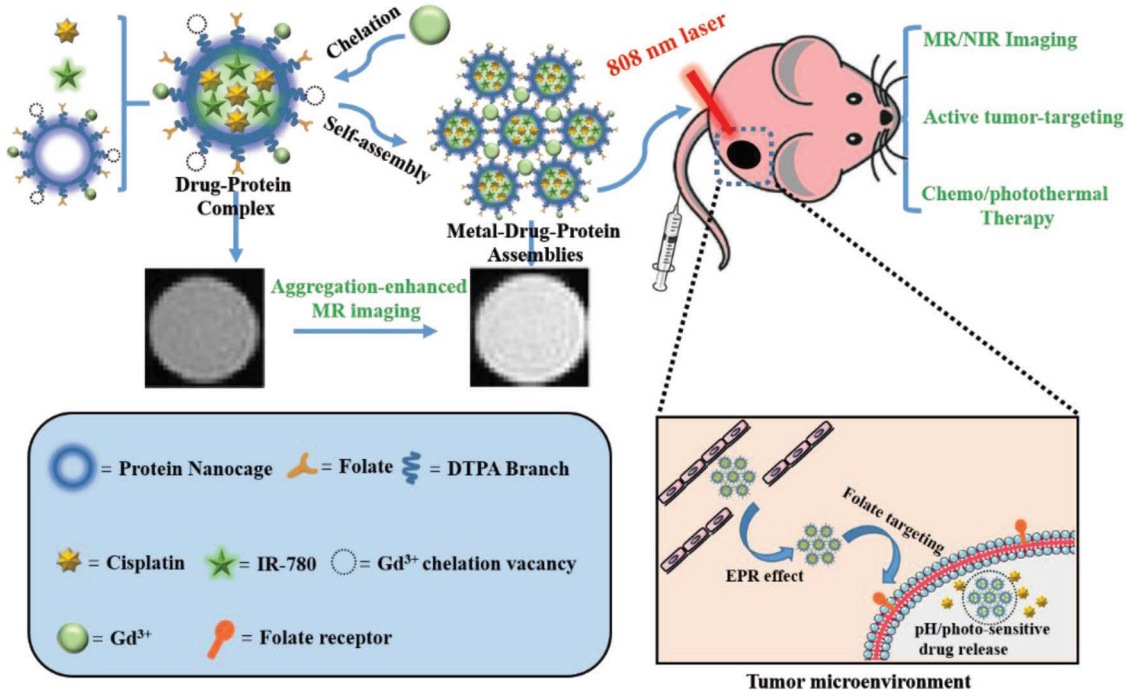

Scheme 1. Fabrication of Gd-P-ABs and the therapy mechanism of Gd-P-ABs

inorganic nanoparticle stabilizer,[10,28] etc. Among them, metal ion–induced protein assembly aroused extensive interest and research. Due to the abundant COOH− group and NH_2− group in protein structure, many kinds of protein could be induced into nanosized assembly via the chelation effect with metal ions (e.g., Gd^{3+}, Mn^{2+}, Cu^{2+}, Ca^{2+}, Fe^{3+}, and Ni). The incorporation of metal ions usually endowed the protein nanosystems' unique functions, such as MR contrast imaging,[29,30] enzyme-like activity,[31] enhanced intracellular entrance,[32] and protein encapsulation.[33,34] However, via a simple chelation effect between metal ions with COOH− group or NH_2− group, these metal–protein assemblies usually faced with uncontrolled assembly process and inhomogeneous size.[29] To overcome the uncertainty, embedded special chelation group into the protein structure tends to prompt "condensed" protein assemblies.[35]

Inspired by the above strategies, a kind of Gd^{3+}–protein assemblies (Gd-P-ABs) with self-enhanced MR imaging capacity were synthesized (**Scheme 1**). Gd-P-ABs loading with cisplatin and IR-780 dye were employed for dual-mode imaging–guided chemo-/photothermal therapy (PTT). In the design progress, folate and Gd-DTPA-modified BSA (folic acid (FA)-^{Gd}BSA) was prior synthesized according to the previous protocol.[36] IR-780 dye and cisplatin were then encapsulated by FA-^{Gd}BSA via the hydrophobic effect. Nanosized assemblies were induced via the chelation effect of Gd^{3+} (52.69 ± 8.48 nm). Notably, the MR longitudinal (r_1) value of Gd-P-ABs further increased to a larger r_1 value (26.391 s^{-1} mM^{-1}) than FA-^{Gd}BSA. Such a fantastic phenomenon probably benefits from aggregation-induced T_1-weighted MR imaging enhancement. When exposed to the acidic tumor microenvironment and external light irradiation, Gd-P-ABs behaved like a responsive drug release, which assisted good therapeutic effects to gastric cancer MGC-803 cells. Moreover, MR/fluorescence (FL) imaging in vivo both revealed that the Gd-P-ABs exhibited high-sensitive tumor-targeting ability and long tumor retention time. A combined therapeutic effect in vivo demonstrated that Gd-P-ABs realized outstanding therapeutic efficacy. Therefore, this work offered a simple approach to fabricate multifunctional protein-based theranostics agents for cancer.

2. Results and Discussion

2.1. Self-Assembly and Characterization of Gd-P-ABs

Gd-DTPA-modified BSA (^{Gd}BSA) was synthesized according to our pervious literature. Due to strong paramagnetism of Gd^{3+}, ^{Gd}BSA was endowed with the function of T_1-weighted MR contrast imaging. Folate was then conjugated to the structure of ^{Gd}BSA (FA-^{Gd}BSA). As we all know, folate has been widely used as targeting molecule due to various kinds of tumors processing high-expressed folate receptor; thus, FA-^{Gd}BSA was endowed with active tumor targeting ability. To form the Gd^{3+}-modulated protein-assemblies, as shown in **Figure 1**a, FA-^{Gd}BSA was used as a protein nanocage to encapsulate IR-780 dye and cisplatin via the hydrophobic effect, forming the protein complex. Considering that there are still some chelation binding sites existing in the structure of FA-^{Gd}BSA (such as Diethylenetriaminepentaacetic acid (DTPA) section and carboxyl group), free Gd^{3+} was proportionally added. Consequently, Gd^{3+} further induced the protein complex self-assembled into uniform nanoparticles (Gd-P-ABs) via the chelation effect. Transmission electron microscopy (TEM) images demonstrated that the Gd-P-ABs were self-assembled into micelles (Figure 1b).

Next, the dynamic light scattering (DLS) data showed that the size of Gd-P-ABs was 52.69 ± 8.48 nm (Figure 1c) with a

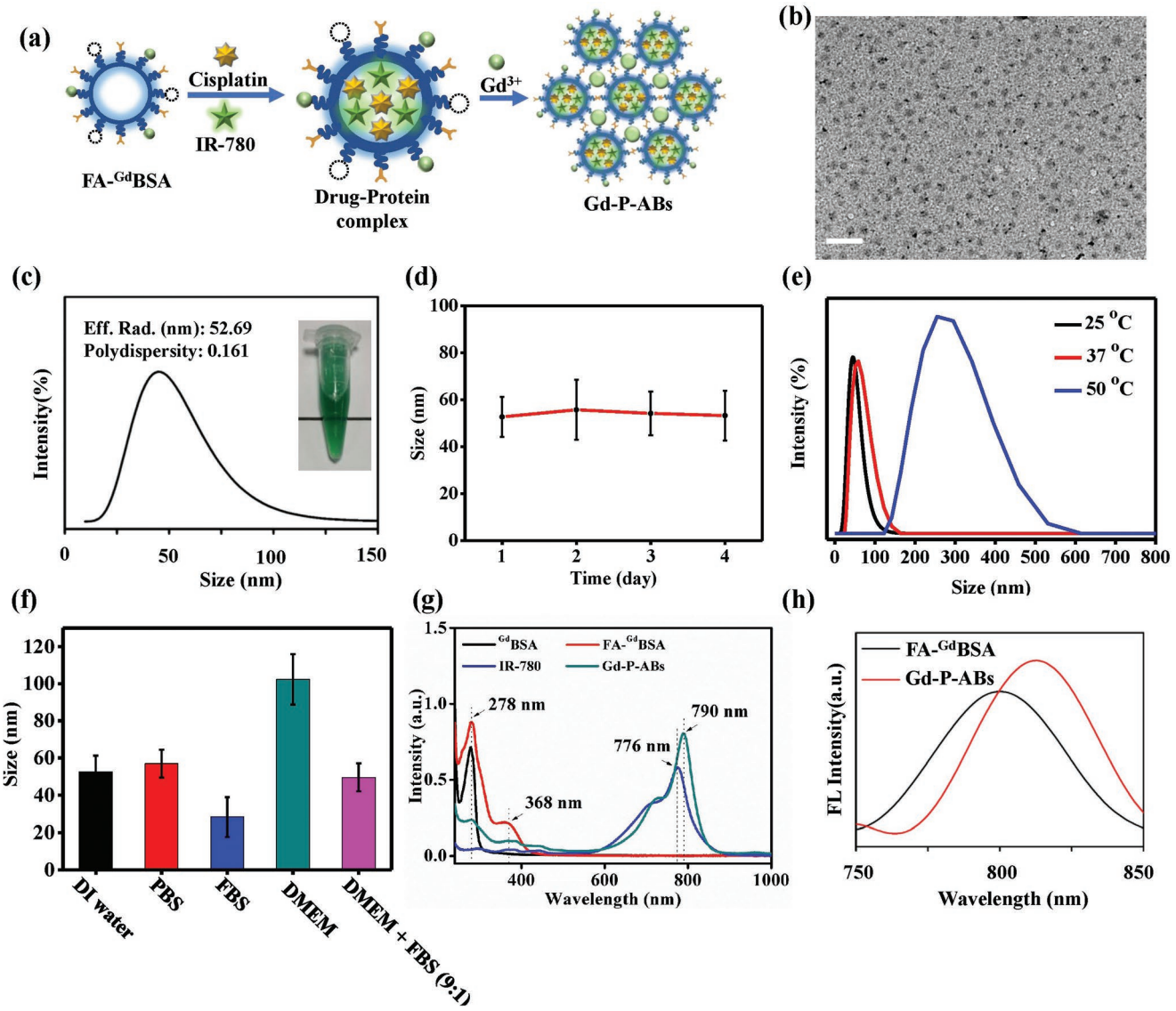

Figure 1. Fabrication and characterization of Gd-P-ABs. a) fabrication process of Gd-P-ABs. b) TEM images of Gd-P-ABs (scale bar: 200 nm). c) Size distribution of Gd-P-ABs (insertion and visual observation of Gd-P-Abs' solution). d) Size fluctuation of Gd-P-ABs within 4 days. e) Size distribution of Gd-P-ABs at 25, 37, and 50 °C. f) Size fluctuation of Gd-P-ABs at different media. g) FL spectrum curves. h) UV–vis spectrum curves.

ζ-potential of –13.35 mV (Figure S1, Supporting Information). The stability of Gd-P-ABs was monitored within 4 days. As shown in Figure 1d, negligible size fluctuation was observed from Gd-P-ABs, which indicated that Gd-P-ABs possessed long-term stability. The thermal stability of Gd-P-ABs was monitored at 25, 37, and 50 °C after incubation for 3 h. As shown in Figure 1e, when subjected to different temperatures, the Gd-P-ABs exhibited good thermodynamic stability at room temperature (25 °C) and body temperature (37 °C) according to the DLS data, but when maintained at 50 °C, the size of Gd-P-ABs caused dramatic expansion, which is mainly because high temperature broke the combined structure of Gd-P-ABs and induced the protein degeneration. Furthermore, size fluctuation of Gd-P-ABs dispersed in different media was observed, as shown in Figure 1f; the size of Gd-P-ABs dispersed in phosphate buffer solution (PBS) or Dulbecco's modified Eagle's Medium (DMEM) + fetal bovine serum (FBS) was similar with deionized (DI) water, whereas obvious change is happened in size when dispersed in FBS or DMEM. The phenomenon indicated that Gd-P-ABs could disassemble in the FBS medium and crosslinking at DMEM. Even though, Gd-P-ABs still maintain relative stability at DMEM + FBS, which demonstrated that Gd-P-ABs could have stability at physiological condition. Notably, when excess Gd^{3+} was added, the protein complex crosslinking happened (Figure S2, Supporting Information), with the ζ-potential being changed from –13.35 to 7.69 mV (Figure S1, Supporting Information). In addition, in order to confirm the existing of Pt and Gd ions in the structure of Gd-P-ABs, elemental analysis by energy dispersive X-ray spectroscopy (EDS) was carried out; the results confirmed that Pt and Gd ions were all existed (Figure S3, Supporting Information). To further confirm that Gd-P-ABs were successfully self-assembled, UV–vis spectra were recorded to determine the formulation; as shown in Figure 1g, the absorption peak of

folate at 365 nm appeared in the spectrum of FA-^{Gd}BSA, which indicated that FA was conjugated to ^{Gd}BSA successfully. The characteristic peak of IR-780 dye with a broad absorption peak between 600 and 900 nm also existed in the spectrum of Gd-P-ABs, which verified that IR-780 was encapsulated by FA-^{Gd}BSA. Furthermore, the bathochromic shift of IR-780 $Q(I)$ band to 790 nm compared with the absorption of free IR-780 dye at 776 nm indicated the environment of IR-780 dye changed. Compared with free IR-780 dye, FL spectrum showed that the emission peak shift from 790 to 825 nm when IR-780 dye was incorporated into the structure of the Gd-P-ABs (Figure 1h); this phenomenon further confirmed that IR-780 dye was combined with FA-^{Gd}BSA.

The r_1 relaxation time was measured and recorded by the 1.41 T minispec mq 60 NMR analyzer (Bruker, Germany); as shown in **Figure 2**a, the r_1 relaxation value of FA-^{Gd}BSA reached to 15.233 s^{-1} mM^{-1} whereas Gd-P-ABs has a higher r_1 relaxation value of 26.391 s^{-1} mM^{-1}. T_1-weighted MR performance in vitro contrastively demonstrated that Gd-P-ABs performed much brighter MR signal than FA-^{Gd}BSA with the same concentration of Gd^{3+} (Figure 2b). Furthermore, a brighter MR signal of Gd-P-ABs was contrastively observed by using a 3.0 T MRI scanner with an animal coil. Thus, the MRI results indicated that Gd-P-ABs exhibited aggregation-enhanced MRI capacity when FA-^{Gd}BSA was self-assembled via the chelation effect of Gd^{3+}. Such a phenomenon should be explained that more Gd^{3+} integration increased the local concentration of Gd^{3+} and lowered the molecular tumbling rate of FA-^{Gd}BSA (Figure 2c,d).[37,38]

Afterward, the photothermal effect was then evaluated. Due to the incorporation of IR-780 dye into the structure of Gd-P-ABs, photo–heat conversion efficiency was prior evaluated by monitoring the temperature changes under laser irradiation. During the irradiation (1.2 W cm^{-2}, 6 min) time, the temperature increased at 9 and 19 °C at a maximum degree

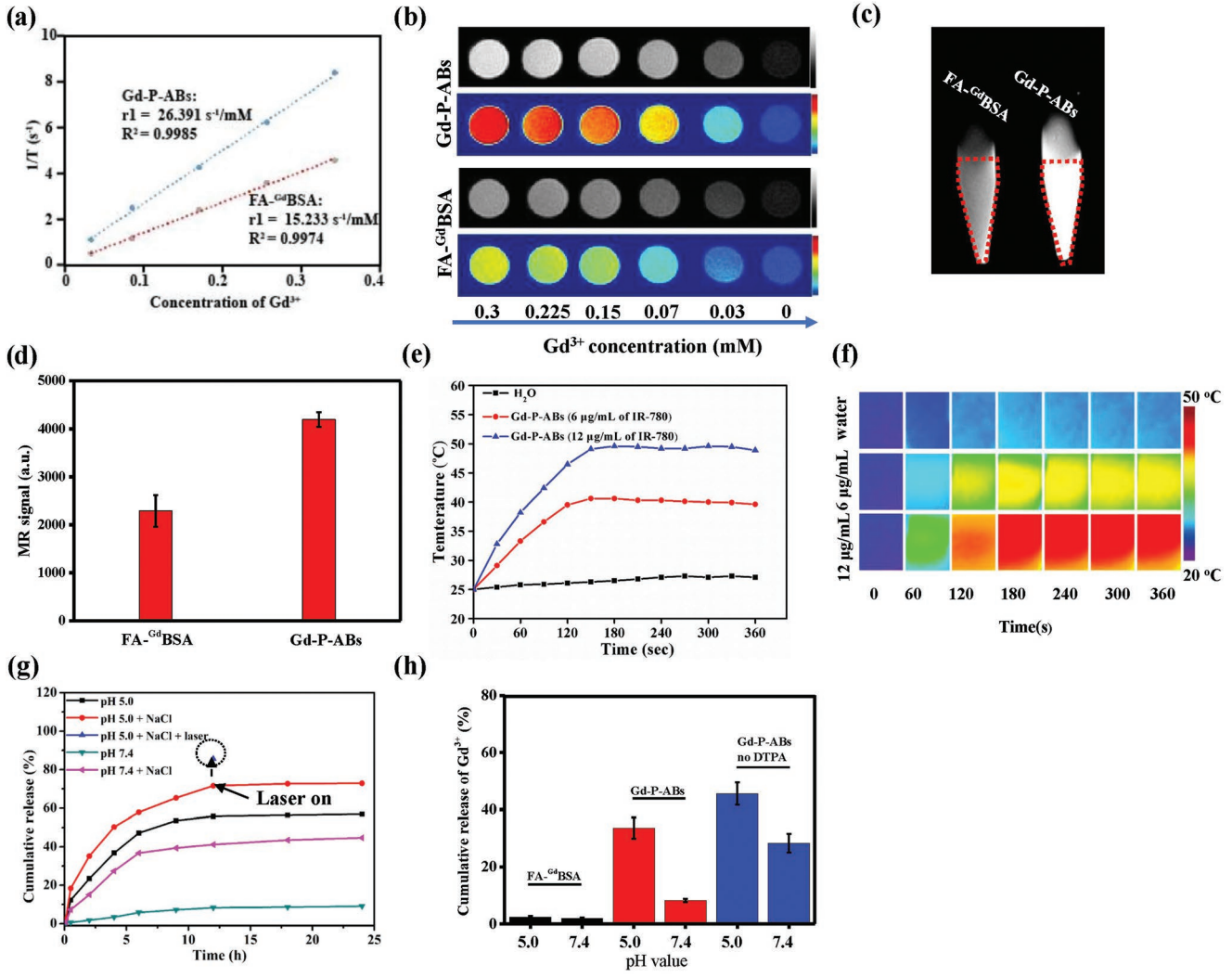

Figure 2. Characterization of Gd-P-ABs. a) r_1 relaxion time of Gd-P-ABs and FA-^{Gd}BSA. b) T_1-weighted MR images (0.5 T) of Gd-P-ABs and FA-^{Gd}BSA. c) T_1-weighted MR images (3.0 T) of Gd-P-ABs and FA-^{Gd}BSA. d) MR signal quantitation of Gd-P-ABs and FA-^{Gd}BSA from panel (c). e) The temperature fluctuation curves of Gd-P-ABs and FA-^{Gd}BSA at different concentrations of IR-780 under laser irradiation; water was used as control. f) Thermal images of Gd-P-ABs and FA-^{Gd}BSA. g) Drug release behaviors of Gd-P-ABs at different stimuli conditions. h) Gd ions' release behaviors at different pH conditions.

when IR-780 dye concentration varied from 6 to 12 μg mL^{-1} (Figure 2e). In contrast, the temperature of water only changed negligibly. The temperature change process was directly monitored by heat relaxation profile (Figure 2f); the results indicated that Gd-P-ABs can act as a good PTT agent.

The cisplatin release capacity was measured when the Gd-P-ABs were dialyzed against different simulative solution environment. As shown in Figure 2g, when Gd-P-ABs were subjected to the physiological condition (pH 7.4), low amount of Pt ions tends to release, indicating the good stability in the blood circulation. However, when Gd-P-ABs were subjected to an acidic condition (pH 5.0), the Pt ions dramatically released with a ratio of 56.9%. Gd-P-ABs exhibited acid-sensitive drug release capacity, which is mainly because the H^+ induced the protonation of carboxylic groups. Cisplatin is sensitive to Cl^-; when Cl^- was added, the Pt ions further released from Gd-P-ABs, which is mainly because excess Cl^- competitively broke the coordination between cisplatin and FA-^{Gd}BSA (COOH group). Consequently, the release ratio of Pt ions reached to 72.9% at acidic condition plus NaCl within 24 h, which is much higher than physiological condition plus NaCl. Furthermore, when a laser irradiation (1.2 W cm^{-2}, 6 min) was added at 12 h, more amount of Pt ions (85.6%) was triggered to release, which is mainly because the light-induced heat broke the combined structure of Gd-P-ABs. Therefore, Gd-P-ABs exhibited pH-/light-responsive drug release.

Furthermore, the Gd ion release behaviors were investigated. As shown in Figure 2h, when incubated at pH 5.0 or pH 7.4, there were almost no Gd ions released from FA-^{Gd}BSA due to the strong chelation effect between Gd and DTPA. However, obvious Gd ions released from Gd-P-ABs at pH 5.0 and 7.4 when DTPA section was absent, whereas no obvious Gd ions released from Gd-P-ABs at pH 7.4 when DTPA section was conjugated to BSA. Notably, obvious Gd ions released from Gd-P-ABs at pH 5.0 even DTPA section was existing. TEM images of Gd-P-ABs at pH 5.0 exhibited that the clear nanostructures disappeared (Figure S4, Supporting Information), which is mainly because acidic pH induced the protonation of carboxylic groups and broke the interaction between cisplatin and FA-^{Gd}BSA (COOH group).

2.2. In Vitro Interaction of Gd-P-ABs

In vitro cell targeting and cellular uptake ability of Gd-P-ABs were carried out. IR-780 dye can emit red fluorescence in NIR I section; the FL image of Gd-P-ABs was thereby captured. As shown in **Figure 3**a, Gd-P-ABs presented distinct red fluorescence compared with water, which indicated that Gd-P-ABs can be further used for the in vivo FL image.

Next, cellular uptake ability of Gd-P-ABs was monitored by confocal laser scanning microscopy (CLSM). Folate-targeting ability of Gd-P-ABs in vitro was administrated by incubation with cancer cells, MGC-803 cells, and normal cells, GES-1 cells. MGC-803 cells presented a stronger red fluorescence signal than GES-1 cells after 1 h incubation (Figure 3b). Meanwhile, MGC-803 cells have more efficient endocytosis to Gd-P-ABs than free IR-780 (Figure S5, Supporting Information). All the results suggesting that the Gd-P-ABs can be specially binding to MGC-803 cell rather than GES-1 cells due to the folate targeting.

Following, the endocytosis of Gd-P-ABs for MGC-803 cells was visually observed by CLSM (Figure 3c). MGC-803 cells emitted brighter red fluorescence signal when the cells treated with Gd-P-Abs, whereas MGC-803 cells emitted weaker brighter red fluorescence signal when the folate molecule of Gd-P-ABs was absent, the results further indicated that the folate molecule plays an important role to endow Gd-P-Abs' special targeting ability with the MGC-803 cells.

Encouraged by the good cellular uptake of Gd-P-ABs, the cytotoxicity study was then administrated. The cytotoxicity in vitro was then evaluated by Cell Counting Kit (CCK-8) assay when the pH values of culture medium were adjusted to 7.4 and 5.0, respectively (Figure 3d). Lowest cell viability can be observed when cells treated with the Gd-P-ABs (pH 5.0) compared with Gd-P-ABs (pH 7.4) or free cisplatin. Additionally, the relative contribution of cell necrosis versus apoptosis was detected by flow cytometry (Figure 3e). A higher apoptosis-to-necrosis ratio was observed when cells were treated with the Gd-P-ABs at pH 5.0 than pH 7.4, suggesting the greater chemotherapy capacity of Gd-P-ABs presented at pH 5.0. All the results predicted that once the Gd-P-ABs get accessed into the tumor site, Pt ions can efficiently release from Gd-P-ABs to kill the cancer cells.

Next, when laser irradiation was added, the cell viability was evaluated by CCK-8 assay. As shown in Figure 3f, the cells treated with the Gd-P-ABs presented much lower cell viability than cells treated with IR-780 dye; the same phenomenon can also be observed by the photodamage images (Figure 3g). Drug loading (DL) values of IR-780 and cisplatin were 5.5% and 4.3%, respectively. According to the results of Figure 3d,f, Gd-P-ABs demonstrated synergistic tumor cell-killing effect with the addition of chemotherapy and photothermal therapy. Therefore, the results demonstrated that the assemblies behaved a superior therapeutic efficacy due to the integrative effect of chemotherapy and photothermal therapy.

2.3. In Vivo MR/FL Imaging

The outstanding performance in vitro encouraged us to monitor the tumor targeting of Gd-P-ABs. First, FL imaging in vivo was carried out by administration of Gd-P-ABs. As shown in **Figure 4**a, the whole mouse body presented brighter fluorescence signal at 2 h postinjection than preinjection. With time prolonging, the tumor site began to present distinct fluorescence signal at 6 h and maintained strong fluorescence signal until 24 h. Notably, the brightest fluorescence signal in tumor site can be observed at 12 h (Figure 4b). Eventually, the background fluorescence signal of mouse body decreased over time but remained clearly legible at the tumor site until 48 h postinjection. The result demonstrated that the Gd-P-ABs can efficiently accumulate to the tumor site. In contrast, when folate was absent from Gd-P-ABs, a delayed tumor accumulation and short retention time was observed. The phenomenon demonstrated that Gd-P-ABs presented active tumor-targeting ability and folate mediated a better tumor targeting of Gd-P-ABs. Meanwhile, ex vivo fluorescence imaging also confirmed the

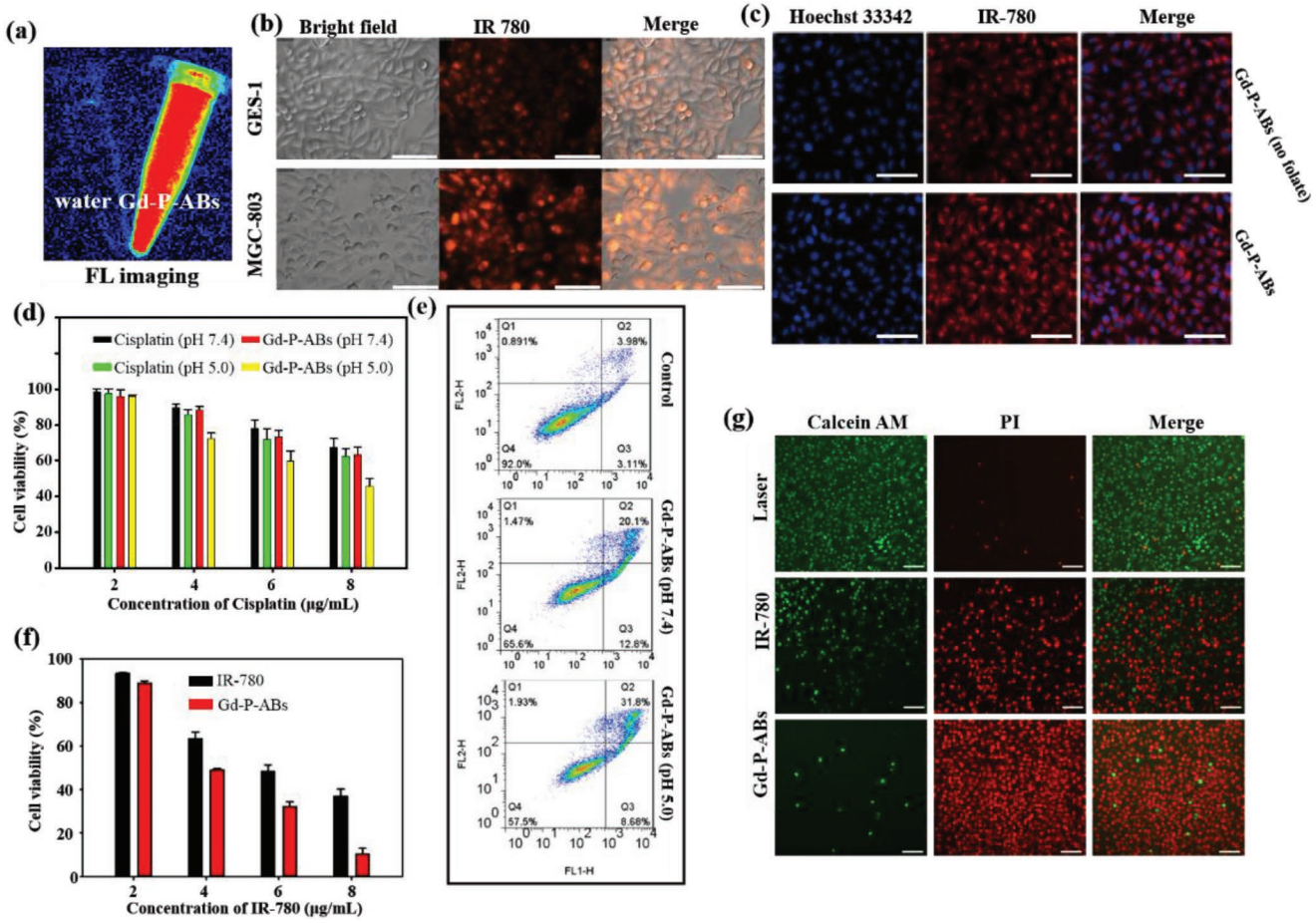

Figure 3. In vitro cellular uptake and cytotoxicity of Gd-P-ABs. a) FL images of Gd-P-ABs and water. b) CLSM images of MGC-803 cells and GES-1 cells incubated with Gd-P-ABs for 1 h (scale bar: 100 μm). c) CLSM images of MGC-803 cells incubated with Gd-P-ABs and Gd-P-ABs with no folate, respectively (scale bar: 100 μm). d) Cell viability of MGC-803 cells incubated with Gd-P-ABs at pH = 7.4 or 5.0. e) Cell necrosis versus apoptosis of MGC-803 cells incubated with Gd-P-ABs at pH = 7.4 or 5.0, measured by flow cytometry assays. f) Cell viability of MGC-803 cells incubated with Gd-P-ABs and IR-780 under laser irradiation. g) Live and death distribution CLSM images of MGC-803 cells after treated with laser, IR-780 + laser, and Gd-P-ABs + laser; green color (Calcien AM) represents live cells and red color (PI) represents death cells (scale bar: 100 μm).

long tumor accumulation behaviors of Gd-P-ABs (Figure 4c; Figure S6, Supporting Information).

Encouraged by the aggregation-enhanced MRI capacity of Gd-P-ABs, in vivo T_1-weighted MR imaging was administrated to evaluate the tumor targeting of Gd-P-ABs. MGC-803 tumor-bearing mice were injected into Gd-P-ABs and FA-^{Gd}BSA, respectively, via tail vein. As shown in Figure 4d, the MR signal intensity of the tumor site presented more and more strong within 720 min postinjection compared with preinjection, and remarkably heightened at 720 min (Figure 4f). Eventually, the tumor site became weaken at 1440 min due to the metabolism of Gd^{3+}. In contrast, mouse treated with FA-^{Gd}BSA cannot be seen with remarkably heightened MR signal in the tumor site. The MR signal even became distinctly weak at 120 min. Notably, when Gd^{3+} was set to a same concentration, a much brighter MR signal could be seen in mouse treated with Gd-P-ABs than mouse treated with FA-^{Gd}BSA. Altogether, the Gd-P-ABs not only presented aggregation-enhanced MRI capacity in vivo but also long tumor accumulation ability. Furthermore, the incorporation of DTPA section was indeed enhanced by the stability of Gd-P-ABs in blood (Figure S7, Supporting Information).

2.4. In Vivo Combined Therapy

Encouraged by the superior therapeutic efficacy in vitro and efficient tumor accumulation capacity, the in vivo tumor inhibition of Gd-P-ABs was comparatively administrated. At first, the photo–heat conversion in vivo was evaluated via thermal imaging. The MGC-803 tumor-bearing mice were injected by a solution containing with free IR-780 or Gd-P-ABs, and the tumor site was subjected by an 808 nm laser (1.2 W cm^{-2}) for 6 min after 12 h postinjection. During the irradiation time, the temperature was recorded by an infrared camera to evaluate the photothermal therapeutic efficacy. As shown in **Figure 5**a, the Gd-P-ABs induced a higher temperature than free IR-780. Such better photothermal therapeutic efficacy of the Gd-P-ABs was predicted to make a more serious injury to tumor tissue. Consequently, the tumor site treated with Gd-P-ABs + laser

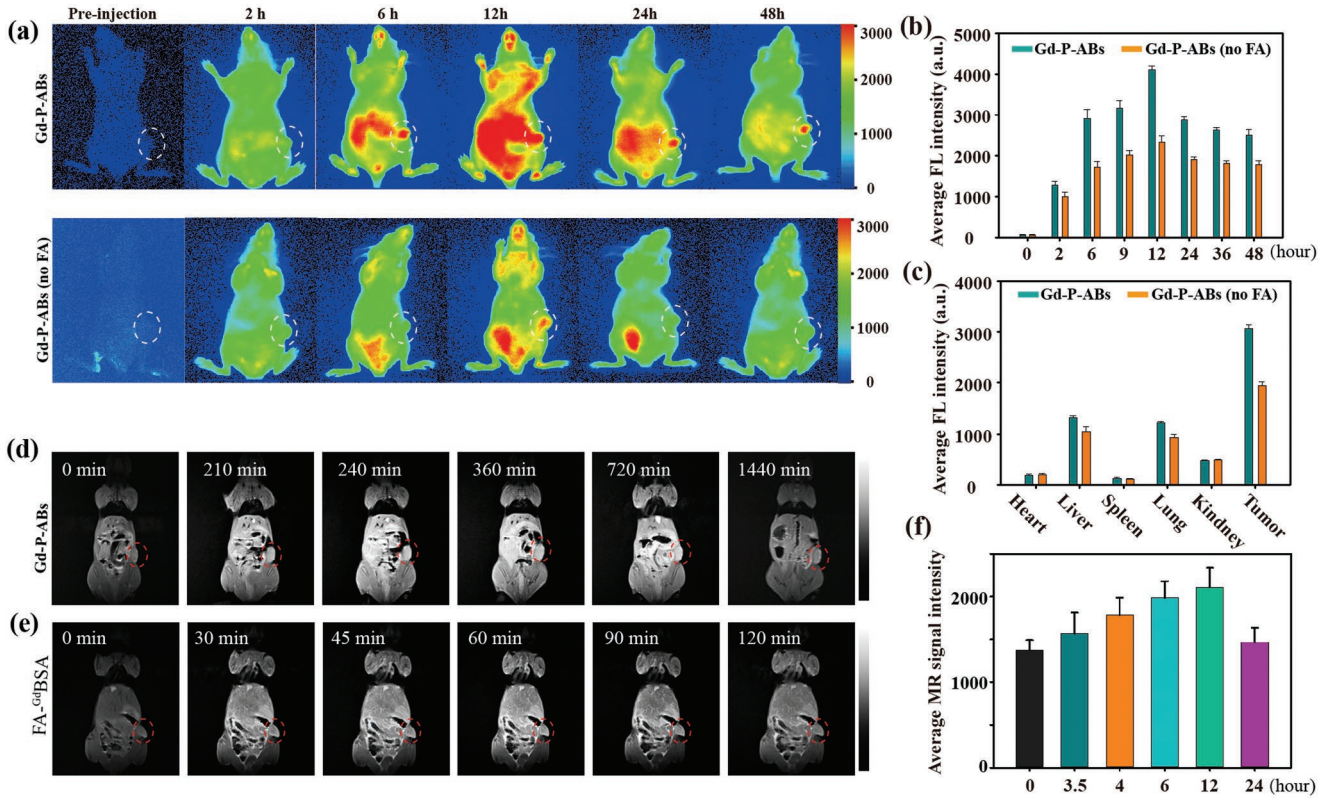

Figure 4. In vivo FL/MR imaging. a) In vivo FL images of mice treated with Gd-P-ABs and Gd-P-ABs with no folate, respectively at different times. b) Average FL intensity of the tumor site at different times. c) Ex vivo average FL intensity of the main organs and tumor. d) In vivo T_1-weighted MR imaging of Gd-P-ABs within 1440 min. e) In vivo T_1-weighted MR imaging of FA-^{Gd}BSA within 120 min. f) Average MR intensity of the tumor site at different times.

became a whole necrotic scar tissue and eventually disappeared without recurrence within 18 days, whereas the tumor treated with IR-780 increased to a large volume even subjected a hemorrhagic injury (Figure 5b). The similar phenomenon could be observed according to the hematoxylin-eosin (H&E)-stained section of tumor (Figure 5c). The chemotherapeutic efficacy was comparatively evaluated. MGC-803 tumor-bearing mice were injected cisplatin or Gd-P-Abs, respectively. As shown in Figure 5b,d, the tumor volume only increased to 3.1 times expansion in a group of Gd-P-ABs whereas 4.8 times in the cisplatin group. As a control, the tumor volume got maximum expansion in the PBS or laser group. Altogether, the Gd-P-ABs exhibited better therapeutic efficacy compared with free IR-780 or free cisplatin. Furthermore, body weight of mice was all slightly increased within 18 days (Figure 5e). H&E-stained organs' section indicated that the Gd-P-ABs have no obvious damage for liver, heart, spleen, kidney, and lung (Figure 5f), which further confirmed that Gd-P-ABs can act as a safe delivery agent.

3. Conclusion

We have successfully fabricated a kind of multifunctional metal–protein assemblies loading with anticancer drug cisplatin and photosentisizer IR-780. Due to the involvement of Gd^{3+}, the as-prepared Gd-P-ABs exhibited aggregation-enhanced T_1-weighted MRI capacity. Such a fantastic feature indicated that Gd-P-ABs can act as an excellent MRI contrast agent. Furthermore, when exposed to simulative environment, the Gd-P-ABs presented tumor-/light-responsive drug release capacity. Excellent tumor cell-targeting and cell-killing performance was confirmed by in vitro CLSM and CCK-8 assays. In vivo MR images demonstrated that the assemblies showed enhanced T_1-weighted MR imaging capacity after self-assembled from Gd^{3+}. Dual MR-/FL-imaging results confirmed that the Gd-P-ABs exhibited active selective tumor accumulation and long retention time. Due to the active tumor-targeting ability of the Gd-P-ABs, better chemo-/photothermal therapeutic performance was observed with the tumor eventually ablation within 18 days. Such excellent performance confirmed the great value of the metal–drug–protein assemblies for cancer theranostics.

4. Experimental Section

Materials: BSA, triethylamine (TEA), and anhydrous dimethyl sulfoxide (DMSO) were purchased form Aladdin Chemistry Co., Ltd (Shanghai, China). *N,N′*-Dicyclohexylcarbodiimide (DCC) and *N*-hydroxysuccinimide (NHS) were purchased from Merck Chemicals Co., Ltd (Shanghai, China). Folate, IR-780 iodide, and gadolinium(III) nitrate hexahydrate ($Gd(NO_3)_3{\cdot}6H_2O$) were purchased from J&K Chemical Ltd (Shanghai, China). Diethylenetriaminepentaacetic acid dianhydride (DTPAA) and cisplatin were obtained from Sam Chemical Technology Co., Ltd (Shanghai, China). Annexin V-fluorescein

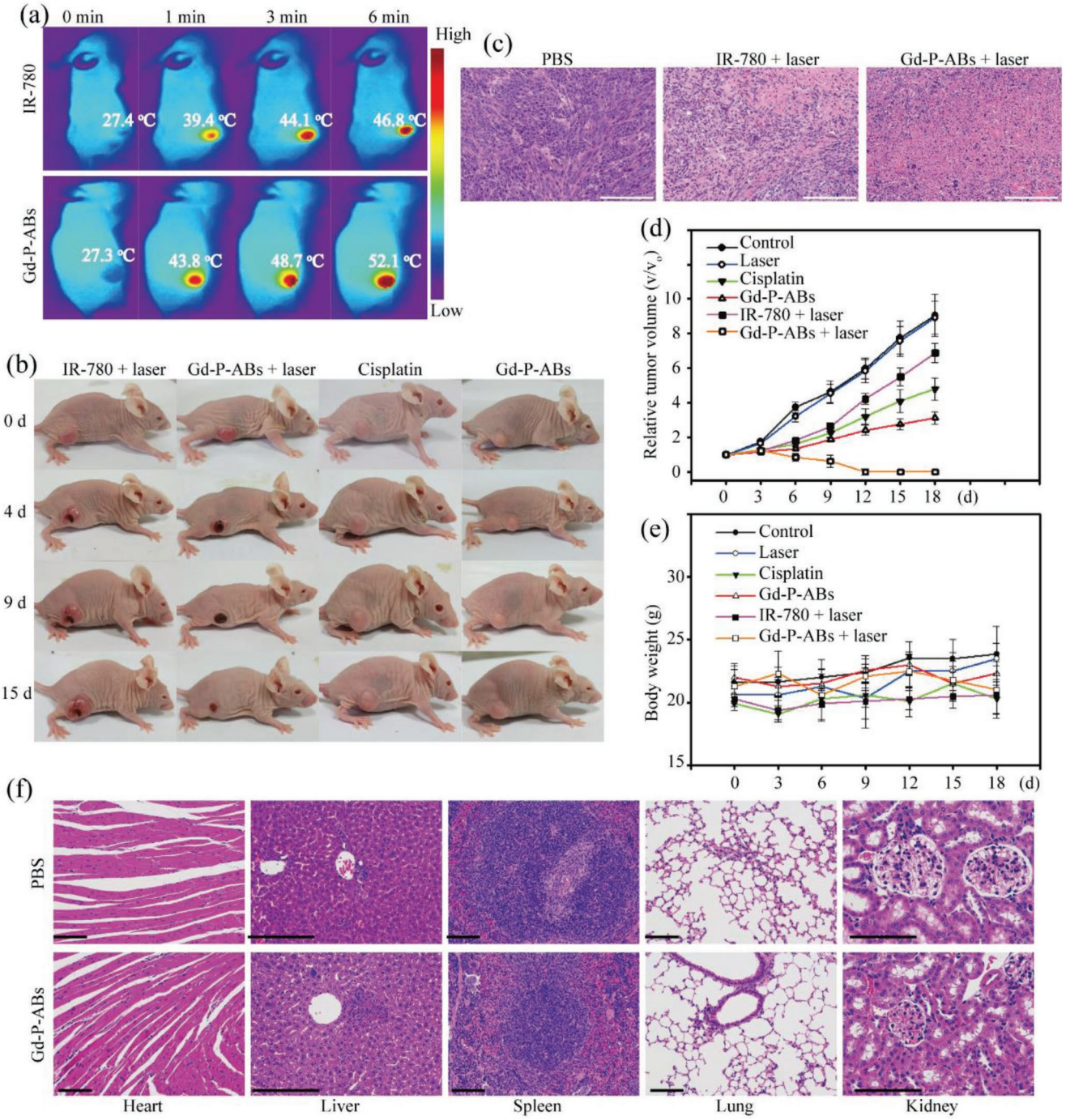

Figure 5. In vivo therapy. a) In vivo heat images of mice treated with IR-780 and Gd-P-Abs, respectively, under laser irradiation. b) Visual observation of therapeutic effect in vivo. c) H&E-stained section of tumor at 6 days. d) The curves of relative tumor volume. e) The curves of body weight. f) Histomorphology observation of main organs (H&E-stained section) (scale bar: 100 μm).

isothiocyanate (Annexin V-FITC)/propidium iodide (PI) apoptosis detection kit, CCK-8, and calcein-AM/PI double stain kit were purchased from Yeasen Corporation (Shanghai, China). Hoechst 33 342 was purchased from Sigma Chemical Corporation (USA). All other chemicals were of reagent grade. Water was purified with a Milli-Q Plus 185 water purification system (Millipore, Bedford, MA, USA).

Synthesis of Modified BSA: ^{Gd}BSA was prior synthesized according to the previously published protocol. Folate was then selected as a targeting molecule to conjugate to ^{Gd}BSA (FA-^{Gd}BSA) via an easy protocol. Briefly, 133 mg of folate was dissolved in 6 mL of anhydrous DMSO containing 60 μL of TEA, and 70 mg of NHS and 66 mg of DCC were then added, respectively. After stirring in the dark for 12 h, the reacted solution was filtered via filtration to remove the insoluble dicyclohexylurea. The above NHS-activated folate solution was added drop wise into 100 mL ^{Gd}BSA (500 mg) aqueous solution under stirring overnight. After that, the reaction solution was filtered via filtration and dialyzed against $NaHCO_3$ solution (0.1 M) and deionized water, respectively. Finally, the purified FA-^{Gd}BSA was obtained via frozen dry.

Preparation of Gadolinium-Modulated Protein Assemblies (Gd-B-ABs): In a typical experiment, 200 µL of DMSO containing 2 mg of IR-780 and 3 mg of cisplatin was added into 4 mL of DI water containing 30 mg of FA-^{Gd}BSA under vigorous stirring. Following, the formed green transparent solution was centrifuged by using ultrafiltration device (100 kDa) and dispersed in 4 mL of citrate buffer (10×10^{-3} M). The dispersed solution was then drop wise added to 600 µL $Gd(NO_3)_3$ solution (6 mg mL^{-1}) and kept stirring for 2 h with the formation of Gd-P-ABs. Finally, the purified Gd-P-ABs were concentrated using ultrafiltration device (100 kDa) and dispersed in deionized water. IR-780 concentration was measured by a UV-vis spectrophotometer, and the Gd^{3+} and Pt^{2+} contents were determined by inductively coupled plasma optical (ICP, Thermo Scientific, iCAP7600).

The entrapment efficiency (EE) and DL were calculated according to the following equations

$$EE(\%) = \left(\left(\text{weight of loaded drug}\right)/\left(\text{weight of initially added drug}\right)\right) \times 100\% \quad (1)$$

$$DL(\%) = \left(\left(\text{weight of loaded drug}\right)/\left(\text{total weight of assemblies}\right)\right) \times 100\% \quad (2)$$

Characterization of the Gd-P-ABs: The size and ξ-potential were measured by dynamic light scattering of NanoBrook Omni Zeta/PLS (Brook, USA). The morphology was observed by a 120 kV Biology transmission electron microscope (Tecnai G2 SpiritBiotwin). The UV–vis spectra were recorded with a Varian Cary 50 spectrophotometer (Varian Inc., Palo Alto, CA, USA). FL spectra were recorded on a Hitachi FL-4600 spectrofluorometer. The r_1 relaxation times were determined by using the 1.41 T minispec mq 60 NMR analyzer (Bruker, Germany).

Photo–Heat Conversion Effect: The dispersed solution of the Gd-P-ABs with different IR-780 concentrations was irradiated by an 808 nm laser at a power density of 1.2 W cm^{-2} for a certain time in a centrifuge tube. Deionized water was irradiated as a control. The temperature changes at different times were monitored by an infrared camera and analyzed using IR Flash Thermal Imaging Analysis software.

In Vitro FL /MR Imaging: The in vitro FL images of Gd-P-ABs were captured using a Bruker In-Vivo F PRO imaging system at different times (Billerica, MA, USA) (excitation at 710/20 nm; emission at 790/30 nm; exposure time being 20 s). Water was used as a control. The in vitro MR images of Gd-P-ABs and FA-^{Gd}BSA with different concentrations of Gd^{3+} were obtained using an MRI system (0.5 T, MesoMR23-060H-I; Shanghai Niumag Corporation, China), respectively.

Drug Release Measurement: The Gd-P-ABs (10 mg mL^{-1}, 2 mL) sealed in a dialysis bag (3500 g mol^{-1}) were dialyzed in different simultaneous solutions (pH 7.4, pH, 5.0, pH 7.4 + NaCl (0.9%), and pH 5.0 + NaCl (0.9%)) at 37 °C. The cumulative release ratio of Pt^{2+} was analyzed by ICP within 24 h. Meanwhile, when the Gd-P-ABs were dialyzed in a solution (pH 5.0 + NaCl (0.9%)) for 12 h, laser irradiation (1.2 W cm^{-2}, 6 min) was added and centrifuged via ultrafiltration device, and the cumulative release ratio of Pt^{2+} was also analyzed by ICP.

Cellular Experiments: The MGC-803 cells cultured in DMEM (HyClone) supplemented with 10% (v/v) FBS (Gibco) at 37 °C (5% CO_2) were selected for cell studies.

The specific folate-targeting ability of the Gd-P-ABs was evaluated by incubation with cancer and normal cells, respectively. MGC-803 and GES-1 cells (5×10^3 cells per well) were cultured in a 96-well plate to adhere for 24 h. A fresh medium containing the Gd-P-ABs was then added to replace the medium. After incubated for 1 h, the cells were washed with PBS for twice and observed by a fluorescence microscope.

To study the cellular uptake of the Gd-P-ABs, MGC-803 cells (1×10^4 cells per well) were cultured in a 4-well chambered bottom dish for 24 h. After incubated with the Gd-P-ABs for a certain time, the cells were washed with PBS twice, and the cells were stained with Hoechst 33 342 and then imaged by a confocal laser scanning microscope (TCS SP8).

For the cell-killing efficacy of the Gd-P-ABs, MGC-803 cells (5×10^3 cells per well) were cultured in 96-cell plates until adherent and then incubated in a fresh medium (pH 7.4 or 5.0) containing cisplatin and Gd-P-ABs with a different concentration, respectively, for 12 h. After washing with PBS twice and incubated for another 6 h, the cell viabilities relative to control cells were determined by the CCK-8 assays. Furthermore, The Annexin V-FITC/PI apoptosis detection kit was employed for apoptotic and necrotic cell distribution. Briefly, MGC-803 cells were cultured in a 12-cell plate (1×10^5 cells per well) to adhere, then the medium was replaced with fresh medium (pH 7.4 or 5.0) containing cisplatin and Gd-P-ABs ([Cisplatin] = 8 µg mL^{-1}), respectively. After incubated for 12 h, the cells were washed twice with PBS, trypsinized, and collected and strained by Annexin V-FITC/PI apoptosis detection kit for fluorescence activated cell sorting (FACS) measurement. The data were analyzed by using FlowJo software 7.6.1.

The photocytotoxic of Gd-P-ABs was also evaluated by CCK-8 assays. MGC-803 cells (5×10^3 cells per well) were cultured in 96-cell plates until adherent and then incubated a fresh medium containing IR-780 and Gd-P-ABs with a different concentration, respectively, for 12 h. After washing with PBS twice, the cells were exposed to an 808 nm laser (1.2 W cm^{-2}, 6 min) and incubated for another 6 h; the cell viabilities relative to control cells were determined by the CCK-8 assays.

The photodamage effect was visually observed by a fluorescence microscope. MGC-803 cells (1×10^4 cells per well) were cultured in a 24-well plate to adhere, and then the medium was replaced with a fresh medium containing IR-780 and the Gd-P-Abs, respectively ([IR-780] = 8 µg mL^{-1}). After incubated for 12 h, the cells were washed with PBS twice and exposed to an 808 nm laser (1.2 W cm^{-2}, 6 min) in the same well. Finally, the cells were stained with Calcein-AM (2.0×10^{-6} M) and PI (1.5×10^{-6} M) and observed by a fluorescence microscope.

Animal Model: Female BALB/c-nude mice (5 weeks old, 18–22 g) were purchased from Shanghai Jiesijie Laboratory Animal Co., Ltd. All animals received care in compliance with the Institutional Animal Care and Use Committee of Shanghai Jiao Tong University. MGC-803 tumor-bearing mice were established by injecting 2×10^6 of MGC-803 cells into the right flank subcutaneously. The tumors were allowed to grow for 10–14 days to reach a volume of ≈100 mm^3 for the in vivo or ex vivo experiment.

In Vivo MR/FL Imaging: For MR imaging in vivo, the MGC-803 tumor-bearing mice were injected with 150 µL of PBS containing Gd-P-ABs and FA-^{Gd}BSA (0.8 mg kg^{-1} of Gd^{3+} to total mouse body weight) via tail vein, respectively. The T_1-weighted MR imaging of the tumor site was monitored and performed on a 3.0 T MRI scanner with an animal coil (MAGENTOM, Verio, Siemens Healthcare, Erlangen, Germany). The sequence was set as the follows: repetition time (TR)/echo time (TE) = 1200/12 ms; acquisition matrix = 256 × 256; field of view = 100 × 100 mm; number of slices = 12, slice thickness = 2 mm, and flip angle = 150°.

For FL imaging in vivo, the mice were injected with 150 µL of PBS containing the protein assemblies and IR-780 (1.2 mg kg^{-1} of IR-780 to total mouse body weight) via tail vein, respectively. The mice were captured using a Bruker In-Vivo F PRO imaging system at different times (Billerica, MA, USA) (excitation at 710/20 nm; emission at 790/30 nm; exposure time being 60 s). The mice were sacrificed by cervical vertebra dislocation after postinjection for 48 h, and the tumor and organs including heart, liver, spleen, lung, and kidney were imaged with the same parameters. The average fluorescence intensity of tumors and organs was quantified by using Bruker Molecular Imaging Software.

In Vivo Stability of Gd-P-ABs: To investigate the stability of Gd-P-ABs, the Gd content in blood was monitored after a mouse was injected with the Gd-P-ABs and Gd-P-ABs with no DTPA (1.5 mg kg^{-1} of Gd to total mouse body weight). The blood was collected from the orbit when Gd-P-ABs was injected via tail vein at different times. The Gd content was analyzed by ICP.

In Vivo Combined Therapy: MGC-803 tumor-bearing mice were intravenously injected with 150 µL of PBS containing cisplatin, IR-780, and the protein assemblies (2.0 mg kg^{-1} of IR-780 and 2.67 mg kg^{-1} of cisplatin to total mouse body weight). After 12 h postinjection, the tumor sites of mice treated with IR-780 and the protein assemblies were irradiated by 808 nm laser (1.2 W cm^{-2}, 6 min). The temperature changes and the infrared images were recorded using an infrared

camera. Following, all the mice were monitored in tumor volume and body weight every 3 days within 18 days. Notably, Tumor volume was calculated via the formulation of (maximum length) × (minimal width)^2 × 1/2. Eventually, the mice were sacrificed, and the organs (e.g., tumor, heart, liver, spleen, lung, and kidney) were excised for further morphological features investigation after H&E staining. Mice treated with PBS were regarded as contrast group.

Supporting Information

Supporting Information is available from the Wiley Online Library or from the author.

Acknowledgements

J.Z. and T.L. contributed equally to this work. This study was supported by the National Basic Research Program of China (Grant Nos. 2010CB933901 and 2015CB931802), the National Key Research and Development Program of China (Grant No. 2017FYA0205301), the National Natural Science Foundation of China (Grant No. 81571835), Shanghai Municipal Commission of Economy and Informatization Technology Fund (Grant No. XC-ZXSJ-02-2016-05), the Shanghai key discipline of medical imaging (Grant No: 2017ZZ02005), the medical engineering cross project of Shanghai Jiaotong university (Grant No. YG2016ZD10).

Conflict of Interest

The authors declare no conflict of interest.

Keywords

aggregation-induced MRI enhancement, chemo-/phototherapy, gadolinium, metal–drug–protein assemblies, MR/FL imaging

Received: October 25, 2019
Revised: January 7, 2020
Published online:

[1] C. L. Degen, M. Poggio, H. J. Mamin, C. T. Rettner, D. Rugar, *Proc. Natl. Acad. Sci. USA* **2009**, *106*, 1313.
[2] Y.-W. Jun, J.-H. Lee, J. Cheon, *Angew. Chem., Int. Ed.* **2008**, *47*, 5122.
[3] T.-H. Shin, Y. Choi, S. Kim, J. Cheon, *Chem. Soc. Rev.* **2015**, *44*, 4501.
[4] M. Miyazaki, V. S. Lee, *Radiology* **2008**, *248*, 20.
[5] K. M. L. Taylor, J. S. Kim, W. J. Rieter, H. An, W. Lin, W. Lin, *J. Am. Chem. Soc.* **2008**, *130*, 2154.
[6] U. I. Tromsdorf, O. T. Bruns, S. C. Salmen, U. Beisiegel, H. Weller, *Nano Lett.* **2009**, *9*, 4434.
[7] Y. Cao, D. Q. Huang, G. Shih, M. R. Prince, *Am. J. Roentgenol.* **2016**, *206*, 414.
[8] J. Ramalho, R. C. Semelka, M. Ramalho, R. H. Nunes, M. AlObaidy, M. Castillo, *Am. J. Neuroradiol.* **2016**, *37*, 1192.
[9] L. D. Weberling, P. J. Kieslich, P. Kickingereder, W. Wick, M. Bendszus, H.-P. Schlemmer, A. Radbruch, *Invest. Radiol.* **2015**, *50*, 743.
[10] X. Xing, B. Zhang, X. Wang, F. Liu, D. Shi, Y. Cheng, *Biomaterials* **2015**, *48*, 16.
[11] W. Hou, F. Xia, G. Alfranca, H. Yan, X. Zhi, Y. Liu, C. Peng, C. Zhang, J. M. de la Fuente, D. Cui, *Biomaterials* **2017**, *120*, 103.
[12] Y. Wang, T. Yang, H. T. Ke, A. J. Zhu, Y. Y. Wang, J. X. Wang, J. K. Shen, G. Liu, C. Y. Chen, Y. L. Zhao, H. B. Chen, *Adv. Mater.* **2015**, *27*, 3874.
[13] Q. Chen, L. Feng, J. Liu, W. Zhu, Z. Dong, Y. Wu, Z. Liu, *Adv. Mater.* **2016**, *28*, 7129.
[14] T. Liu, C. Wang, X. Gu, H. Gong, L. Cheng, X. Shi, L. Feng, B. Sun, Z. Liu, *Adv. Mater.* **2014**, *26*, 3433.
[15] C. Wang, L. Cheng, Z. Liu, *Biomaterials* **2011**, *32*, 1110.
[16] S. Fang, J. Lin, C. Li, P. Huang, W. Hou, C. Zhang, J. Liu, S. Huang, Y. Luo, W. Fan, D. Cui, Y. Xu, Z. Li, *Small* **2017**, *13*, 1602580.
[17] M. Ahmed, L. Solbiati, C. L. Brace, D. J. Breen, M. R. Callstrom, J. W. Charboneau, M.-H. Chen, B. I. Choi, T. de Baere, G. D. Dodd III, D. E. Dupuy, D. A. Gervais, D. Gianfelice, A. R. Gillams, F. T. Lee Jr., E. Leen, R. Lencioni, P. J. Littrup, T. Livraghi, D. S. Lu, J. P. McGahan, M. F. Meloni, B. Nikolic, P. L. Pereira, P. Liang, H. Rhim, S. C. Rose, R. Salem, C. T. Sofocleous, S. B. Solomon, M. C. Soulen, M. Tanaka, T. J. Vogl, B. J. Wood, S. N. Goldberg, *Radiology* **2014**, *273*, 241.
[18] Z. Sheng, D. Hu, M. Zheng, P. Zhao, H. Liu, D. Gao, P. Gong, G. Gao, P. Zhang, Y. Ma, L. Cai, *ACS Nano* **2014**, *8*, 12310.
[19] Q. Chen, Z. Liu, *Adv. Mater.* **2016**, *28*, 10557.
[20] A. Srivatsan, J. R. Missert, S. K. Upadhyay, R. K. Pandey, *J. Porphyrins Phthalocyanines* **2015**, *19*, 109.
[21] Y.-J. Kim, B. Kim, D. C. Hyun, J. W. Kim, H.-E. Shim, S.-W. Kang, U. Jeong, *Macromol. Chem. Phys.* **2015**, *216*, 1161.
[22] H. S. Ryu, K. S. Hong, J. K. Lee, D. J. Kim, J. H. Lee, B. S. Chang, D. H. Lee, C. K. Lee, S. S. Chung, *Biomaterials* **2004**, *25*, 393.
[23] G. Zheng, X. Liu, X. Wang, L. Chen, H. Xie, F. Wang, H. Zheng, W. Yu, X. Ma, *Macromol. Biosci.* **2014**, *14*, 655.
[24] A. O. Elzoghby, W. M. Samy, N. A. Elgindy, *J. Controlled Release* **2012**, *157*, 168.
[25] F. Kratz, *J. Controlled Release* **2008**, *132*, 171.
[26] T. L. Li, J. Zhou, C. L. Zhang, X. Zhi, J. Q. Niu, H. L. Fu, J. Song, D. X. Cui, *NPG Asia Mater.* **2018**, *10*, 1046.
[27] T. Yang, Y. A. Tang, L. Liu, X. Y. Lv, Q. L. Wang, H. T. Ke, Y. B. Deng, H. Yang, X. L. Yang, G. Liu, Y. L. Zhao, H. B. Chen, *ACS Nano* **2017**, *11*, 1848.
[28] M. Mikhaylova, D. K. Kim, C. C. Berry, A. Zagorodni, M. Toprak, A. S. G. Curtis, M. Muhammed, *Chem. Mater.* **2004**, *16*, 2344.
[29] H. M. Yuan, C. Xu, Y. Zhao, B. R. Yu, G. Cheng, F. J. Xu, *Adv. Funct. Mater.* **2016**, *26*, 2855.
[30] Q. Chen, X. Wang, C. Wang, L. Feng, Y. Li, Z. Liu, *ACS Nano* **2015**, *9*, 5223.
[31] T. L. Li, J. Zhou, L. R. Wang, H. F. Zhang, C. F. Song, J. M. de la Fuente, Y. X. Pan, J. Song, C. L. Zhang, D. X. Cui, *Adv. Healthcare Mater.* **2019**, *8*, 1900192.
[32] L. Wang, C. Zhang, T. Li, M. Duan, F. Xia, X. Li, C. Song, S. Pan, B. Liu, D. Cui, *Nanoscale* **2019**, *11*, 22237.
[33] M. B. van Eldijk, L. Schoonen, J. Cornelissen, R. J. M. Nolte, J. C. M. van Hest, *Small* **2016**, *12*, 2476.
[34] C. Yuan, J. Chen, S. Yu, Y. Chang, J. Mao, Y. Xu, W. Luo, B. Zeng, L. Dai, *Soft Matter* **2015**, *11*, 2243.
[35] T. R. Cook, Y. R. Zheng, P. J. Stang, *Chem. Rev.* **2013**, *113*, 734.
[36] J. Zhou, T. Li, C. Zhang, J. Xiao, D. Cui, Y. Cheng, *Nanoscale* **2018**, *10*, 9707.
[37] P. Caravan, Z. D. Zhang, *Eur. J. Inorg. Chem.* **2012**, *2012*, 1916.
[38] K. M. Bennett, J. Jo, H. Cabral, R. Bakalova, I. Aoki, *Adv. Drug Delivery Rev.* **2014**, *74*, 75.

